HHS Public Access

Author manuscript

*Cancer Nanotechnol*. Author manuscript; available in PMC 2021 July 30.

Published in final edited form as:

*Cancer Nanotechnol*. 2020 ; 11(1): . doi:10.1186/s12645-020-00062-8.

# Doxorubicin-loaded hollow gold nanospheres for dual photothermal ablation and chemoembolization therapy

**Rahul A. Sheth**[1,*], **Xiaoxia Wen**[2], **Junjie Li**[2], **Marites P. Melancon**[1], **Xin Ji**[3], **Y. Andrew Wang**[3], **Cheng-Hui Hsiao**[4], **Diana S-L. Chow**[4], **Elizabeth M. Whitley**[5], **Chun Li**[2], **Sanjay Gupta**[1]

[1]Department of Interventional Radiology, The University of Texas MD Anderson Cancer Center, Houston, TX 77030, USA.

[2]Department of Cancer Systems Imaging, The University of Texas MD Anderson Cancer Center, Houston, TX 77030, USA.

[3]Ocean Nanotech, San Diego, CA 92126, USA.

[4]Department of Pharmacological and Pharmaceutical Sciences, College of Pharmacy, University of Houston, Houston, Texas 77030, USA.

[5]Department of Veterinary Medicine & Surgery, The University of Texas MD Anderson Cancer Center, Houston, TX 77030, USA.

## Abstract

**Background—**Doxorubicin-loaded hollow gold nanospheres (Dox@HAuNS) are a promising technology for simultaneous trans-arterial tumor-targeted chemotherapy delivery and thermal ablation. We evaluated the efficacy of intra-arterial delivery of Dox@HAuNS followed by photothermal ablation (PTA) in a rabbit model of liver cancer. Adult New Zealand white rabbits (N=25) were inoculated with VX2 tumors into the left lobe of the liver. The animals were then randomized to sham surgery (N=5), PTA only (N=3), Dox@HAuNS only (N=5), HAuNS + PTA (N=5), and Dox@HAuNS + PTA (N=7). Nanoparticles were delivered as an emulsion with Lipiodol (Guerbet, France) via a trans-arterial approach. Following nanoparticle delivery, PTA was performed using an 808nm fibered laser at 1.5W for 3 minutes. Thermography during PTA demonstrated a sustained elevation in tumoral temperature in both HAuNS + laser and Dox@HAuNS + laser treatment groups relative to animals that underwent laser treatment without prior nanoparticle delivery.

[*]Corresponding author: Rahul Sheth, Department of Interventional Radiology, The University of Texas MD Anderson Cancer Center, Houston, TX 77030, USA, Tel: (713) 745-0652, rasheth@mdanderson.org.

Authors' contributions: XW, JL, MM, XJ, AW, and CL contributed to study design, nanoparticle synthesis, data analysis, and manuscript writing. CH and DC performed doxorubicin quantification and also contributed to data analysis and manuscript writing. EMW performed tissue histology preparation and analysis as well as manuscript writing. RAS and SG performed the in vivo experimentation and imaging analysis as well as contributed to manuscript writsing. All authors read and approved the final manuscript.

Ethics approval and consent to participate: All animal experiments were carried out in accordance with the European Convention for the Protection of Vertebrate Animals (Strasbourg 1986). All animal experimentation was approved by the Institutional Animal Care and Use Committee.

Availability of data and materials: The datasets used and/or analysed during the current study are available from the corresponding author on reasonable request.

Conflicts of interest: The authors declare no potential conflicts of interest.

**Results—**There was a significant decrease in tumor volumes in all three treatment arms relative to control arms ($P = 0.004$). Concentrations of intratumoral doxorubicin were significantly greater in animals treated with laser compared to those that were not treated with laser ($P < 0.01$).

**Conclusions—**Doxorubicin-loaded HAuNS is a promising therapeutic agent for dual ablation/chemoembolization treatment of liver cancer.

### Keywords

gold nanoparticles; drug delivery; thermal ablation; hepatocellular carcinoma; transarterial delivery

## Background

Transarterial chemoembolization (TACE) and thermal ablation are cornerstones in the management of hepatocellular carcinoma (HCC). Both are incorporated into the most commonly used treatment guidelines and are considered the standard of care for early-stage and intermediate stage HCC. Ablation of small (less than 3 cm) tumors is accepted as an alternative to surgical resection, and TACE has demonstrated improvements in overall survival for intermediate stage HCC. In 2002, both Llovet et al. (1) and Lo et al. (2) published randomized trials demonstrating survival advantages with TACE over embolization alone and conservative management, respectively. This level 1 evidence led to the incorporation of TACE as standard of care for patients with intermediate stage HCC by the Barcelona Clinic Liver Cancer (BCLC) system. However, as experience with these procedures has grown over the past three decades, it has become clear that the complete eradication of tumor is not always possible with these individual approaches. For ablation, incomplete lesion coverage or the presence of marginal micrometastases can lead to residual or recurrent tumor (3). For TACE, microenvironmental barriers to drug delivery diminish treatment efficacy (4).

Thermal ablation and TACE affect cell death by orthogonal methods, but these approaches can be complementary. Embolization can increase overall ablation zone size, and ablation can kill tumor cells far from blood vessels that are insensitive to TACE. Indeed, several clinical trials have shown improvements in outcomes when TACE and ablation are performed simultaneously (5,6). While such results are promising, ultimately any combinatorial approach is still constrained by the inherent limitations of each individual treatment modality. The ability to achieve high and sustained concentrations of doxorubicin (Dox) within the target lesion while avoiding off-target and systemic toxicity is an important unmet clinical need with TACE. Likewise, in the clinical setting, the goal of thermal ablation is to eradicate the tumor as well as a margin of tissue around the lesion to ensure complete coverage. This is accomplished by a variety of modalities designed to achieve temperatures greater than 60°C (7). At these temperature ranges, ablation has been shown in randomized trials to achieve outcomes similar to surgical resection (8). However, as all conventional ablation methods generate heat in a manner unprejudiced by the type of tissue in which the ablation needle is inserted, potentially serious complications can occur when critical structures are included in the ablation zone. Thus, a tumor-specific ablation modality would represent a significant advancement over the current status quo.

We have previously shown that hollow gold nanoshells (HAuNS) containing Dox (Dox@HAuNS) are effective at achieving ablative temperatures when irradiated with near infrared (NIR) light. In our previous work, we have shown that unlike Dox@HAuNS, Dox-coated solid gold nanoparticles do not respond to NIR laser irradiation to release Dox (9). This suggests that plasmon absorption of the NIR light and subsequent elevation of temperature around DOX@AuNP mediates release of Dox. Changes in HAuNS morphology were observed after NIR laser irradiation, suggesting that this might be partially responsible for NIR laser mediated Dox release. However, other possible mechanisms, such as decreased ionic interaction between Dox and HAuNS, may also play a role. In this manner, HAuNS-based therapy has the potential to eradicate tumoral cells via three simultaneous and tumor-specific insults: ablation, embolization, and chemotherapy. The purpose of this study was to evaluate the effects of HAuNS-mediated localized Dox delivery and photothermal ablation (PTA) on tumor growth when delivered intra-arterially in a rabbit model of liver tumor.

## Results

### Nanoparticle characterization

PEG-HAuNS and Dox@HAuNS nanoparticles were found to be equally efficient in absorbing NIR photons, with a peak absorbance around 800 nm (Fig. 1A). The Dox@HAuNS nanoparticle had an additional secondary peak from 450–550 nm, reflecting the absorbance of the associated Dox. The absorption spectra showed that the plasmon resonance peak for PEG-HAuNS was tuned to the NIR region (780–810 nm). The sizes of both nanoparticles in a hydrated state were 80–90 nm as determined by dynamic light scattering. (Fig. 1B). Transmission electron microscopy (TEM) revealed the morphology of the HAuNS (Figure S1), and indicated that they had a diameter of ~45 nm and a shell thickness of 4–6 nm. The inner diameter of HAuNS was about 35 nm. TEM also revealed change in the morphology of Dox@HAuNS before and after NIR laser irradiation (Figure S2). The concentration of Dox and HAuNS used in both in vitro and in vivo experiments were 0.5 mg Dox/mL. The concentration of Dox was determined by subtracting free Dox from total Dox added to HAuNS solution. Free Dox was measured by UV-Vis absorbance of Dox in supernatant after remove ultracentrifugation to Dox@HAuNS. The concentration of HAuNS was 40 OD (equivalent to 1 mg HAuNS/mL. About 30% of Dox was released from Dox@HAuNS after NIR irradiation at 4 W/cm$^2$ output power for 5 min. However, almost no Dox was released when laser was turned off over a 1-h period. After a second 5-min irradiation cycle, about 60% of Dox was released. These results suggest that Dox release from Dox@HAuNS was triggered by NIR laser.

### Laser-mediated photothermal effects in vivo in N1–S1 HCC in rat liver.

Rats bearing N1–S1 tumors in the liver were used to determine the optimal laser power generated in the absence and presence of PEG-HAuNS after their intraarterial injection. The mean tumor temperature in the presence of PEG-HAuNS delivered intraarterially increased 12.8±0.8 °C, 21.2±2.0 °C, and 38.5±17.2 °C at laser powers of 1.0 W, 1.5 W, and 2.0 W, respectively. In comparison, the mean tumor temperature without HAuNS injection increased 5.3±0.9 °C, 9.1±2.2 °C, and 16.9±1.5 °C at laser powers of 1.0 W, 1.5 W, and 2.0 W, respectively (n = 3). At a power of 1.5W, temperature elevation was < 10°C in the

absence of PEG-HAuNS but increased to be >20°C in the presence of PEG-HAuNS. On the basis of these results, we chose 1.5 W as the laser output power in all our subsequent studies in rabbit with VX2 tumors.

## Intra-arterial delivery and PTA

All rabbits survived trans-arterial delivery of the nanoparticle constructs as well as photothermal ablation procedures. Technical success for endovascular delivery of the nanoparticle-oil emulsion into the proper hepatic artery was 94% (15/17). Technical success for PTA via mini-laparotomy was 100%. However, two animals in the Dox@HAuNS + laser and one animal in the Dox@HAuNS group were euthanized prior to post-operative day 7 (POD7) due to poor oral intake; this was attributed to off-target embolization of the gastroduodenal artery during the endovascular delivery of the nanoparticle-oil emulsion. The remaining 19 animals (control arm [n=5], Dox@HAuNS + laser arm [n=5], Dox@HAuNS only [n=4], PEG-HAuNS + laser [n=5]) comprised the study cohort; an additional 3 rabbits comprised a laser only arm without nanoparticles for determining temperature generation without prior nanoparticle delivery.

Infrared thermography during PTA demonstrated a sustained elevation in tumoral temperature during laser illumination in both HAuNS + laser and Dox@HAuNS + laser treatment groups relative to animals that underwent laser treatment without prior nanoparticle delivery (Fig. 2). Of note, there was increased heat generation in the Dox@HAuNS group compared to the PEG-HAuNS group, although the underlying cause of the difference in heat generation remains to be identified.

Contrast-enhanced CT images at POD7 and POD14 confirmed targeted delivery of the nanoparticle emulsion by illustrating the retained lipiodol and nanoparticles staining around the tumor (Fig. 3A).

The top panel in Figure 3A shows representative images from a control animal, with each time point showing interval growth in the tumor. The middle panel is an animal treated with Dox@HAuNS, and the bottom panel is an animal treated with Dox@HAuNS + laser; both treatment animal CT images demonstrate geographic areas of necrosis with retained lipiodol staining within the tumor vasculature without evidence of residual or recurrent tumor growth.

Tumor volumetric analysis showed no significant difference in tumor volumes at the baseline CT scan on POD1 across the treatment groups (median 0.19 $cm^3$, range 0.06 – 0.58 $cm^3$, $p = 0.4$). However, at both POD7 ($P = 0.004$) and at POD14 ($P = 0.004$), there was a significant difference in tumor volumes between the control arm and all three treatment arms (Fig. 3B, C). There was no significant difference at either POD7 ($P = 0.10$) or POD14 ($P = 0.25$) in tumor volumes among the three treatment arms (Dox@HAuNS alone, PEG-HAuNS + laser, and Dox@HAuNS + laser).

## Analysis of Dox concentrations

The mean concentration of Dox in plasma 1 h after injection of Dox@HAuNS without and with laser treatment was 2.7 and 6.4 ng/mL, respectively (Fig 4A). The concentration of Dox

increased moderately with laser treatment, however, there was large variation in the Dox plasma concentration with laser treatment. Dox was undetectable 1 day after Dox@HAuNS administration with the exception of rabbits in the Dox@HAuNS + laser group, in which Dox in the plasma was detected in 2 of the 5 samples analyzed (1.62; 7.85 ng/mL). These data are consistent with our finding *in vitro* that laser treatment triggered release of Dox (9). All plasma samples collected at POD7 and POD14 had undetectable Dox. Concentrations of Dox within tissue samples from the tumor site at POD14 were significantly greater in animals treated with laser compared to those that were not treated with laser (mean Dox concentration 72.0 ± 14.3 ng/g with laser versus 34.9 ± 6.6 ng/g tissue without laser; $p < 0.01$, Student's t test) (Fig. 4B). On the other hand, laser irradiation upon the tumor did not result in a significant difference in Dox concentration in liver tissues adjacent to the tumor (22.1±10.3 with laser versus 28.4±9.0 ng/g tissue without laser) (Fig. 4B). Likewise, there was no difference in Dox concentration between tumoral tissue that was not treated with laser and the surrounding liver parenchyma (34.9 ± 6.6 versus 28.4 ± 9.0 ng/g).

## Histopathologic analysis

Animals were euthanized at POD14, and tumors were harvested for histolopathologic analysis. VX2 tumor from rabbit liver consist of a moderately well-demarcated, single to multilobular mass comprised of a single, pleomorphic population of polygonal cells in islands, nests, and larger groups subdivided by delicate fibrovascular stroma and central regions of necrosis. A variably intense infiltrate of lymphocytes, plasma cells, and macrophages and zone of fibrosis surrounds tumors (Figure S3).

At POD14, tumor xenografts were present in liver sections from all animals in the control group and in animals treated with laser only, but were not consistently present in liver samples from other treatment groups, including treatments with Dox@HAuNS, HAuNS + laser (PTA alone), and Dox@HAuNS + laser (combined Chemo-PTA) (Supplementary Table S1). Local release of Dox from intra-arterially delivered Dox@HAuNS and PTA mediated laser illumination resulted in significant reduction in mean tumor diameter compared with untreated tumors ($p<0.01$) (Fig. 5A). Tissue responses in liver samples from treated animals include locally extensive ischemic liver necrosis, loss of hepatic cords with retention and collapse of portal structures, and replacement by immature fibrous tissue (post-necrotic collapse and scar tissue formation). Macrophages and multinucleated giant cells surround and infiltrate the margins of necrotic tumor and/or liver and are present in areas of post-necrotic collapse (Fig. 5C–5E). In some samples, nodules of viable VX2 tumor are present (Figs 5C, 5D), whereas in other samples no histological presence of residual tumors could be found (Fig. 5E); tumors without residual disease were found mostly in livers of rabbits treated with Dox@HAuNS + laser.

Nanoparticles were concentrated in areas of tumor. Finely granular, brown-black foreign material (consistent with aggregates of nanoparticles and visualized by silver enhancement) is present in material filling the lumen and lining walls of some arterioles in areas of tissue necrosis and in the cytoplasm of macrophages and giant cells (Fig. 6). As shown in Figure S4 our data clearly delineated the presence of gold nanoparticles in tumors. In tumors not exposed to laser, HAuNS were largely distributed to perivascular zone. In tumors exposed to

laser treatment, HAuNS were present as clusters in large quantity in the necrotic zone (Figure S4). Nanoparticles were also concentrated in areas of adjacent liver, causing necrosis and post-necrotic scarring, presumably owing to embolization caused by Lipiodol/Dox@HAuNS (Figure S5 and S6).

## Discussion

We selectively delivered Dox@HAuNS mixed with ethiodized oil to arterioles of hepatic tumors causing embolization, local release of Dox triggered by laser illumination, and PTA effect, leading to significant reduction and sometimes complete elimination of tumors. We also observed zones of hepatic ischemic necrosis in ablated tumor tissues. Many of the areas of necrosis are centered on an arteriole containing nanoparticles Dox@HAuNS or PEG-HAuNS. Selective distribution of nanoparticles to tumor arteriole should reduce the potential for off-target thermal injury. Thus, this combination of therapies resulted in effective tumor killing. Moreover, we demonstrated that the application of photothermal energy results in a significant increase in the intra-tumoral concentration of Dox, but not in adjacent peritumoral liver tissue. This was because the normal liver was not in the direct path of laser beam and thus release of Dox from Dox@HAuNS was not triggered by the laser (9). Laser-triggered Dox release was also evidenced by higher plasma Dox concentration observed at 1 h after laser illumination in rabbits received intraarterial injection of Dox@HAuNS compared to rabbits received Dox@HAuNS treatment alone. A benefit of this approach is that targeted, local delivery of Dox may reduce the potential for systemic toxicity including doxorubicin-mediated cardiotoxicity (10). Taken together, we have demonstrated that the HAuNS platform is capable of the near-simultaneous, targeted delivery of three orthogonal methods of anti-cancer therapy: embolization, chemotherapy, and thermal ablation.

There is a sound biological rationale for the simultaneous treatment of HCC with both TACE and thermal ablation. Physiologically, pre-ablation embolization reduces the heat sink effect within the tumor and adjacent parenchyma, thus yielding larger ablation zones (11,12). From a tumor heterogeneity perspective, thermal ablation is effective at eradicating cells remote from blood vessels that are conditioned for hypoxic environments and are therefore resistant to the effects of embolization and chemotherapy. In a prospective clinical trial of 139 patients, Peng et al. (6) observed a significant improvement in survival when TACE was combined with thermal ablation for tumors ranging from 3–5cm; no significant difference in outcomes was seen in patients with tumors smaller than 3cm. A subsequent clinical trial of 189 treatment-naïve patients with tumor up to 7cm likewise showed an improvement in overall survival when TACE was combined with ablation relative to ablation alone (5).

Fundamentally, however, the limitations of conventional ablation and embolization techniques restrict the therapeutic efficacy of combination approaches. The effectiveness of particle embolics on the micron size scale to induce significant hypoxia (13) or to deliver Dox at cytotoxic concentrations (14) is a major concern with current TACE methods. Likewise, the lack of tumor specificity for current thermal ablation technologies can result in insufficient tumor coverage as well as damage to adjacent critical structures.

Photothermal conversion nanoparticles represent a promising technology to address these hurdles. For example, thermally sensitive liposomal constructs containing Dox have been shown to increase intratumoral concentrations of the drug when systemic delivery is combined with thermal ablation in a mouse model (15). While external targeting peptides were used in this liposomal study to increase intratumoral concentrations, there was no difference in survival between animals treated with the targeted or non-targeted liposomal formulations. Also, given the limitations of the animal model used in this study, the more clinically relevant large animal liver tumor models amendable to intra-arterial delivery, as opposed to intravenous delivery, should be tested.

Relative to liposomal nanoparticles, gold nanoparticles have the advantage of intrinsic and efficient heat generation by photon absorption. They are also highly tunable and can operate in the NIR, allowing for maximal optical penetration. These photothermal properties alone have motivated extensive preclinical investigations in the use of gold nanoparticles as a PTA agent (16). Moreover, a pilot study using gold nanoparticles for targeted PTA in patients with head and neck cancer has also been pursued (ClinicalTrials.gov identifier NCT00848042). When formulated into hollow nanoshell constructs, gold nanoparticles (HAuNS) can additionally serve as drug delivery vehicles. Indeed, the drug delivery capabilities of gold nanoparticles forms the foundation of a Phase I clinical trial (17). Hollow gold nanospheres have plasmon absorption tuned in the NIR region and display strong photothermal coupling property suitable for PTA therapy. HAuNS do not have silica core as gold nanoshells have and lack of cytotoxic surfactants that are usually associated with gold nanorods because such surfactants are required for gold nanorod preparation. As a result, PEG-HAuNS are have insignificant toxicity in mice (18). It is possible that other NIR-absorbing materials, such as indocyanine green, may also mediate photothermal effects to kill tumor cells. The advantages of Dox@HAuNS are 2-fold: 1) it displays a greater photothermal conversion efficiency than indocyanine green, 2) Dox release from Dox@HAuNS was triggered by laser exposure, therefore there was greater retention of Dox during laser treatment after Dox@HAuNS administration.

Laser irradiation of HAuNS not only results in ablative temperature generation but also in targeted drug release. In this study, we found a greater than 2-fold increase in tumoral Dox concentrations due to thermally mediated release of Dox from the nanoshells. Moreover, potentially due to the influence of simultaneous embolization with ethiodized oil, this elevation in Dox concentration was measured 14 days following delivery, indicating sustained retention of the drug within the tumors. These results are in agreement with prior studies. For example, Ma et al. (19) demonstrated increased Dox release following NIR illumination of gold-studded nanomicelles. Likewise, we have previously shown that targeted DOX@HAuNS, when combined with NIR illumination, results in significantly improved tumor control relative to HAuNS followed by NIR illumination in a murine model following systemic delivery in mice with ovarian cancer xenografts (20) and in rats with orthotopically inoculated liver cancer following intraarterial administration (3).

Histological examinations revealed that while 3 out of 3 rabbits in the control arm (no treatment plus laser alone) had extensive VX2 tumors in the liver, only 4 of 12 rabbits in the 3 treatment arms (Dox@HAuNS, PEG-HAuNS plus laser, or Dox@HAuNS plus laser) had

residual tumor 14 days after treatment. While we could not find differences among the 3 treatment arms with regards to tumor control, there was a trend towards the lowest diameter of residual viable tumor in the Dox@HAuNS plus laser arm compared to the other 2 treatment arms. Future studies that monitor survival of treated animals as the end point may allow us to separate the Dox@HAuNS plus laser treatment arm from the PTA alone group (HAuNS plus laser) and/or the chemotherapy alone (Dox@HAuNS) group.

We acknowledge several limitations to our study. First, the lack of long-term clearance and toxicity studies for HAuNS in large animals is an important barrier to translation. We have previously investigated the biodistribution, organ elimination, and acute and chronic toxicity of PEG-HAuNS in normal mice (5). We found that PEG-HAuNS caused no adverse effects after 10 daily intravenous injections over a 2-week period at a dose of 12.5 mg/kg per injection (accumulated dose: 125 mg/kg). The dose of PEG-HAuNS used in the current study after a single intraarterial injection in rabbits was 1 mg equivalent Au per rabbit, or about 0.33 mg Au/kg body weight assuming each rabbit weight 3 kg. Such as dose was only 0.26% of the dose used in the previous toxicity study in mice. However, significant quantity of Au was found retained in the liver and spleen in mice 90 days after intravenous injection of PEG-HAuNS. Uptake of HAuNS by macrophages and giant cells in rabbit liver, either through direct phagocytosis of injected nanoparticles, indirectly uptake through cell debris containing HAuNS, or both, was observed 14 days after injection of Dox@HAuNS or PEG-HAuNS. Therefore, it is likely that HAuNS will be retained in the liver for a prolonged period of time in rabbits, as was the case in mice. Given that several pilot and Phase I studies that investigate the safety and toxicity of gold nanoparticles have been initiated, their use will hopefully become a clinical reality in the near future.

Second, there was a large variation in temperature elevation possibly resulting from variation in laser placement and heterogeneity of tumor physiology, which may be the cause of large variation in plasma Dox concentration measured at 1 h after laser illumination and variation in intratumoral Dox concentration measured at 14 days after laser illumination. Such variation may affect treatment outcome for individual rabbits. Future efforts should be made to improve the uniformity of treatment. Transarterial chemo-embolization is the standard of care treatment for HCC. In the clinical setting, embolization is always paired with a chemotherapy agent, as established by all international guidelines. To answer the question of the effect of embolization alone in this animal model, we would need to have a control arm in which only lipiodol was delivered. However, as this is never an option clinically, we did not perform this experiment as it is not clinically relevant.

## Conclusions

This study advances the clinical translational potential of the HAuNS platform by demonstrating both its selective release of Dox and intra-tumoral heat generation. Building upon prior rodent work (20,21), we found that simultaneous stresses of embolization, hyperthermia, and chemotherapy could be delivered via clinically available catheters and via a standard trans-arterial approach. These data support the strong potential clinical utility for Dox@HAuNS as a dual ablation/chemoembolization treatment modality for HCC.

## Methods

### Synthesis and Characterization of Dox@HAuNS

PEGylated hollow gold nanoshells (PEG-HAuNS) were obtained from Ocean NanoTech (San Diego, CA, USA). Briefly, HAuNS were synthesized by the cobalt NP–mediated reduction of chlorauric acid followed by PEGylation as described previously (9). The resulting HAuNS were coated with MeO-PEG5000-SH to yield PEG-HAuNS. For Dox loading, 0.5 mL of Dox (OChem Inc., Des Plaines, IL, USA) in water (1 mg/mL) was added to 0.5 mL of PEG-HAuNS (80 OD). The mixture was incubated at 4°C overnight to form Dox@HAuNS. Before injection, 1 ml of Dox@HAuNS solution was thoroughly mixed with 0.4 ml of Lipiodol oil by using two syringes connected to a 3-way Hi-Flo disposable stopcock.

For characterization, the UV-UV-visible spectroscopy was recorded on a Beckman Coulter DU-800 UV-visible spectrometer (Fullerton, CA). The hydrodynamic sizes of PEG-HAuNS and Dox@HAuNS were determined using dynamic light scattering on a Brookhaven 90 plus particle size analyzer (Holtsville, NY). The size of HAuNS in dry state was examined by a JEM-1400 transmission electron microscope operated at 80 kV (JEOL Ltd., Tokyo, Japan).

### Animal models

All animal experimentation was approved by the Institutional Animal Care and Use Committee. Animals were housed in facilities approved by the Association for Assessment and Accreditation of Laboratory Animal Care International and in accordance with regulations and standards of the U.S. Department of Agriculture, the U.S. Department of Health and Human Services, and the National Institutes of Health.

A total of 25 adult New Zealand white rabbits were included in this study. All procedures were performed under anesthesia with isofluorane (5%) in oxygen (1.5L/min) and intramuscular buprenorphine (0.15 mg, Buprenex, Bedford Laboratories, Bedford, OH). For tumor inoculation procedures, the abdomen was shaved and was subsequently prepped and draped in standard sterile fashion. VX2 tumors were implanted into the left hepatic lobe, as previously described (22). Tumors were allowed to grow for 2 weeks, a duration that we have found to consistently result in ~1.0 – 1.5 cm diameter tumors. The rabbits were then randomized to 4 groups: sham surgery (control group, n = 5), intra-arterial Dox@HAuNS only (Dox@HAuNS group, n = 5), intra-arterial Dox@HAuNS followed by laser (Dox@HAuNS + laser, n = 7), and intra-arterial HAuNS followed by laser (HAuNS + laser, n = 5). Three rabbits were randomized to receive laser treatment only as an additional negative control group.

### Intra-arterial delivery of nanoparticles

Transarterial intrahepatic delivery of the nanoparticles was performed via a femoral approach. After achieving adequate anesthesia, the right inguinal region was shaved and then prepped and draped in standard sterile fashion. A 1 cm vertical incision was made in the proximal right femur, and after blunt dissection, the right common femoral artery was isolated. Proximal and distal control was obtained with 0-silk vessel loops. Intra-arterial

access was obtained with a 21g micropuncture needle followed by a 0.016” microwire. The access was then serially dilated to allow for the placement of a 4Fr sheath (Cook Medical, Bloomington, IN). Through this sheath, a 2.8Fr microcatheter (EmboCath Plus; BioSphere Medical, Rockland, MA, USA) was advanced over a 0.014” microwire (Transcend, Boston Scientific, Natick, MA) into the celiac trunk under fluoroscopic guidance. Intermittent digital subtraction angiography was performed to assist in navigating the microcatheter to the proper hepatic artery. The nanoparticle solution (1 mL total volume, 40 OD, 1 mg Au/mL, 0.5 mg Dox/mL) was emulsified in 0.4 mL ethiodized oil (Lipiodol, Guerbet, Aulnay-sous-Bois, France). The emulsion was delivered through the microcatheter at a rate of 0.2 mL per minute under fluoroscopic visualization. After removal of the microcatheter and sheath, the femoral artery was ligated proximally and distally with the previously placed vessel loops.

### Photothermal ablation of hepatic tumors

Immediately following the delivery of the nanoparticles, the skin overlying the abdomen was prepped and draped in standard sterile fashion. A midline incision was made, and the left hepatic lobe was elaborated to the skin. A fiberoptic catheter with a 1 cm diffusing tip (BioTex) was advanced into the tumor under direct visualization. Photothermal ablation was performed with an 808 nm laser at 1.5 watt for 3 minutes. Continuous thermography was performed with an infrared camera (FLIR). The abdomen was then closed with both deep and subcuticular absorbable sutures.

### CT volumetry

Contrast-enhanced CT scans were performed using a helical CT scanner (HiSpeed Advantage; GE Medical Systems, Milwaukee, WI). Imaging was performed on operative day to establish baseline tumor volumes, as well as on post-operative day 7 (POD7) and POD14. Tumor volumes were measured using a standard three-dimensional image analysis software package (iNtuition; TeraRecon, Foster City, CA) based on 1.5 mm slices.

### Histopathologic evaluation

On POD14, the rabbits were euthanized with an overdose of Beuthanasia-D (1.0 mL/10 lb). Tumor and adjacent liver from control (n=3), Dox@HAuNS (n=4), laser alone (n=2), HAuNS + laser (n=4), and Dox@HAuNS + laser (n=5) groups were harvested for analysis. Tissues for histopathology were fixed in 10% neutral buffered formalin, processed using standard protocols, embedded in paraffin, sectioned at 5 microns and stained with hematoxylin and eosin or for nanoparticle visualization. Nanoparticles in tissue sections were highlighted using a silver enhancer kit (ab170733, Abcam), with neutral red (ab146365, Abcam) counterstain to identify lysosomes in phagocytes. Stained tissue sections were evaluated microscopically by a board-certified veterinary pathologist using a Leica DM2500 microscope equipped with a Leica DFC495 digital camera. Residual tumor was quantified by measuring the longest diameter of viable tumor. Each tumor was sampled in triplicate to minimize the risk of sampling bias.

## Quantitative analysis of doxorubicin

Dox levels in each tumor, liver tissue adjacent to tumors, and in plasma were measured by high performance liquid chromatography (HPLC). Plasma samples were collected at 1 h post-operation, POD1, POD7 and POD14. Tumor and liver tissues were harvested on POD14. Blood and tissues collected were kept at −80°C until the time of process. For sample preparation, dissected tissues were weighted and homogenized in water (0.2 gram tissue/mL of water). Dox in the homogenate (0.1 ml) was extracted by using Waters' Oasis HLB solid phase extraction cartridge (Milford, MA. USA) with the following steps: 1) loading of 100 μL homogenates mixed with 1 ml 0.1 N HCl to the cartridge, 2) washing the cartridge with 1 mL water to remove impurities, 3) elution of analytes by 1 mL of acetonitrile, and 4) collection of eluate and evaporation to dryness followed by reconstitution with 20% acetonitrile in water (100 μL). Plasma samples (100 μL) were extracted by adding 0.5 mL of ethyl acetate. After vortexing and centrifugation (15,000 *g* for 15 min), the supernatants were evaporated to dryness and reconstituted with 20% acetonitrile in water (100 μL).

To construct the calibration curve, stock solutions of Dox HCl (1 mg/mL) and daunorubicin HCl (Cayman Chemical, Ann Arbor, MI. USA) (1 mg/mL) were dissolved in water. Working solutions of the analytes were obtained by further diluting the corresponding stock solution with 20% acetonitrile in water. Calibration standard solutions were prepared freshly by spiking in Dox to plasma or homogenized liver/tumor tissues and extracted before each analytical run. At least eight calibration concentrations in the range of 1.5–500 ng/mL for plasma and 1.5–500 ng/mL for liver/tumor (7.5–2,500 ng/gram of tissue) were used to generate the calibration curves for quantifications of unknown samples. All samples and calibration standards contained 100 ng/mL of daunorubicin HCl as the internal standard.

HPLC separation was achieved on a Waters HPLC system equipped with a Model 2475 multi λ Fluorescent Detector and an Eclipse XDB-C18, 5 μm, 4.6 × 150 mm column. Mobile phase was delivered at a flow rate of 1 mL/min with 16 min run time. The mobile phase consisted of water containing 0.1% formic acid (mobile phase A) and acetonitrile containing 0.1% formic acid (mobile phase B). The following gradient was used: 80% of A (0–1 min); 80–65% of A (1–2 min); 65% of A (2–8 min); 65–10% of A (8–9 min); 10% of A (9–13 min); 10–80% of A (13–14 min); 80% of A (14–16 min). The wavelengths of excitation and emission were 480 nm and 560 nm, respectively for fluorescent detection. Injection volume was 80 μl for extracts of liver/tumor homogenates and plasma samples.

## Statistical analysis

All statistical analyses were performed with R (The R Foundation), a free software environment for statistical computing and graphics or Prism 7.03 for Windows (GraphPad Software, La Jolla, CA). Univariate analysis was performed using the Wilcoxon rank sum test. The Kruskal-Wallis test was used to compare percent change in tumor volumes across the treatment groups. One-way ANOVA with Tukey's multiple comparisons test was performed to compare tumor diameters in histologic section. A cutoff value of $P < 0.05$ was used for statistical significance.

## Supplementary Material

Refer to Web version on PubMed Central for supplementary material.

## Funding:

This work was supported in part by the National Cancer Institute (grant R44 CA196025) and by the John S. Dunn Foundation. This research was conducted at the MD Anderson Center for Advanced Biomedical Imaging in-part with equipment support from General Electric Healthcare. We acknowledge the NCI Cancer Center Support Grant P30 CA016672 to MD Anderson Cancer Center for support of the animal studies.

## Abbreviations

| | |
|---|---|
| **HAuNS** | hollow gold nanoshells |
| **Dox** | doxorubicin |
| **Dox@HAuNS** | doxorubicin-loaded hollow gold nanospheres |
| **PEG-HAuNS** | PEGylated hollow gold nanoshells |
| **PTA** | photothermal ablation |
| **TACE** | Transarterial chemoembolization |
| **HCC** | hepatocellular carcinoma |
| **POD** | post-operative day |
| **CT** | computed tomography |

## References

1. Llovet JM, Real MI, Montañá X, Planas R, Coll S, Aponte J, et al. Arterial embolisation or chemoembolisation versus symptomatic treatment in patients with unresectable hepatocellular carcinoma: a randomised controlled trial. Lancet. 2002;359:1734–9. [PubMed: 12049862]
2. Lo C-M, Ngan H, Tso W-K, Liu C-L, Lam C-M, Poon RT-P, et al. Randomized controlled trial of transarterial lipiodol chemoembolization for unresectable hepatocellular carcinoma. Hepatology. 2002;35:1164–71. [PubMed: 11981766]
3. Paulet E, Aubé C, Pessaux P, Lebigot J, Lhermitte E, Oberti F, et al. Factors limiting complete tumor ablation by radiofrequency ablation. Cardiovasc Intervent Radiol. 2008;31:107–15. [PubMed: 17968620]
4. Sheth RA, Hesketh R, Kong DS, Wicky S, Oklu R. Barriers to drug delivery in interventional oncology. J Vasc Interv Radiol. 2013;24:1201–7. [PubMed: 23735316]
5. Peng Z-W, Zhang Y-J, Chen M-S, Xu L, Liang H-H, Lin X-J, et al. Radiofrequency ablation with or without transcatheter arterial chemoembolization in the treatment of hepatocellular carcinoma: a prospective randomized trial. J Clin Oncol. 2013;31:426–32. [PubMed: 23269991]
6. Peng Z-W, Zhang Y-J, Liang H-H, Lin X-J, Guo R-P, Chen M-S. Recurrent hepatocellular carcinoma treated with sequential transcatheter arterial chemoembolization and RF ablation versus RF ablation alone: a prospective randomized trial. Radiology. 2012;262:689–700. [PubMed: 22157201]
7. Kis B, El-Haddad G, Sheth RA, Parikh NS, Ganguli S, Shyn PB, et al. Liver-Directed Therapies for Hepatocellular Carcinoma and Intrahepatic Cholangiocarcinoma. Cancer Control. 2017;24:1073274817729244.

8. Fang Y, Chen W, Liang X, Li D, Lou H, Chen R, et al. Comparison of long-term effectiveness and complications of radiofrequency ablation with hepatectomy for small hepatocellular carcinoma. J Gastroenterol Hepatol. John Wiley & Sons, Ltd; 2014;29:193–200. [PubMed: 24224779]
9. You J, Zhang G, Li C. Exceptionally high payload of doxorubicin in hollow gold nanospheres for near-infrared light-triggered drug release. ACS Nano. 2010;4:1033–41. [PubMed: 20121065]
10. Singal PK, Iliskovic N. Doxorubicin-induced cardiomyopathy. New England Journal of Medicine. 1998;339:900–5.
11. Covey AM, Hussain SM. Liver-Directed Therapy for Hepatocellular Carcinoma: An Overview of Techniques, Outcomes, and Posttreatment Imaging Findings. American Journal of Roentgenology. 2017;209:67–76. [PubMed: 28350491]
12. Tanaka M, Ando E, Simose S, Hori M, Kuraoka K, Ohno M, et al. Radiofrequency ablation combined with transarterial chemoembolization for intermediate hepatocellular carcinoma. Hepatol Res. 2014;44:194–200. [PubMed: 23521520]
13. Levy EB, Gacchina Johnson C, Jacobs G, Woods DL, Sharma KV, Bacher JD, et al. Direct Quantification and Comparison of Intratumoral Hypoxia following Transcatheter Arterial Embolization of VX2 Liver Tumors with Different Diameter Microspheres. J Vasc Interv Radiol. 2015;26:1567–73. [PubMed: 26231108]
14. Minchinton AI, Tannock IF. Drug penetration in solid tumours. Nat Rev Cancer. 2006;6:583–92. [PubMed: 16862189]
15. Yan F, Wang S, Yang W, Goldberg SN, Wu H, Duan W-L, et al. Tumor-penetrating Peptide-integrated Thermally Sensitive Liposomal Doxorubicin Enhances Efficacy of Radiofrequency Ablation in Liver Tumors. Radiology. 2017;285:462–71. [PubMed: 28631963]
16. Hwang S, Nam J, Jung S, Song J, Doh H, Kim S. Gold nanoparticle-mediated photothermal therapy: current status and future perspective. Nanomedicine. 2014;9:2003–22. [PubMed: 25343350]
17. Libutti SK, Paciotti GF, Byrnes AA, Alexander HR, Gannon WE, Walker M, et al. Phase I and Pharmacokinetic Studies of CYT-6091, a Novel PEGylated Colloidal Gold-rhTNF Nanomedicine. Clin Cancer Res. American Association for Cancer Research; 2010;16:clincanres.0978.2010–6149.
18. You J, Zhou J, Zhou M, Liu Y, Robertson JD, Liang D, et al. Pharmacokinetics, clearance, and biosafety of polyethylene glycol-coated hollow gold nanospheres. Part Fibre Toxicol. BioMed Central; 2014;11:26–14.
19. Ma Y, Liang X, Tong S, Bao G, Ren Q, Dai Z. Gold Nanoshell Nanomicelles for Potential Magnetic Resonance Imaging, Light-Triggered Drug Release, and Photothermal Therapy. Advanced Functional Materials. WILEY-VCH Verlag; 2013;23:815–22.
20. You J, Zhang R, Xiong C, Zhong M, Melancon M, Gupta S, et al. Effective photothermal chemotherapy using doxorubicin-loaded gold nanospheres that target EphB4 receptors in tumors. Cancer Res. 2012;72:4777–86. [PubMed: 22865457]
21. Li J, Zhou M, Liu F, Xiong C, Wang W, Cao Q, et al. Hepatocellular Carcinoma: Intra-arterial Delivery of Doxorubicin-loaded Hollow Gold Nanospheres for Photothermal Ablation-Chemoembolization Therapy in Rats. Radiology. Radiological Society of North America; 2016;281:427–35.
22. Tian M, Lu W, Zhang R, Xiong C, Ensor J, Nazario J, et al. Tumor Uptake of Hollow Gold Nanospheres After Intravenous and Intra-arterial Injection: PET/CT Study in a Rabbit VX2 Liver Cancer Model. Mol Imaging Biol. Springer US; 2013;15:614–24. [PubMed: 23608932]

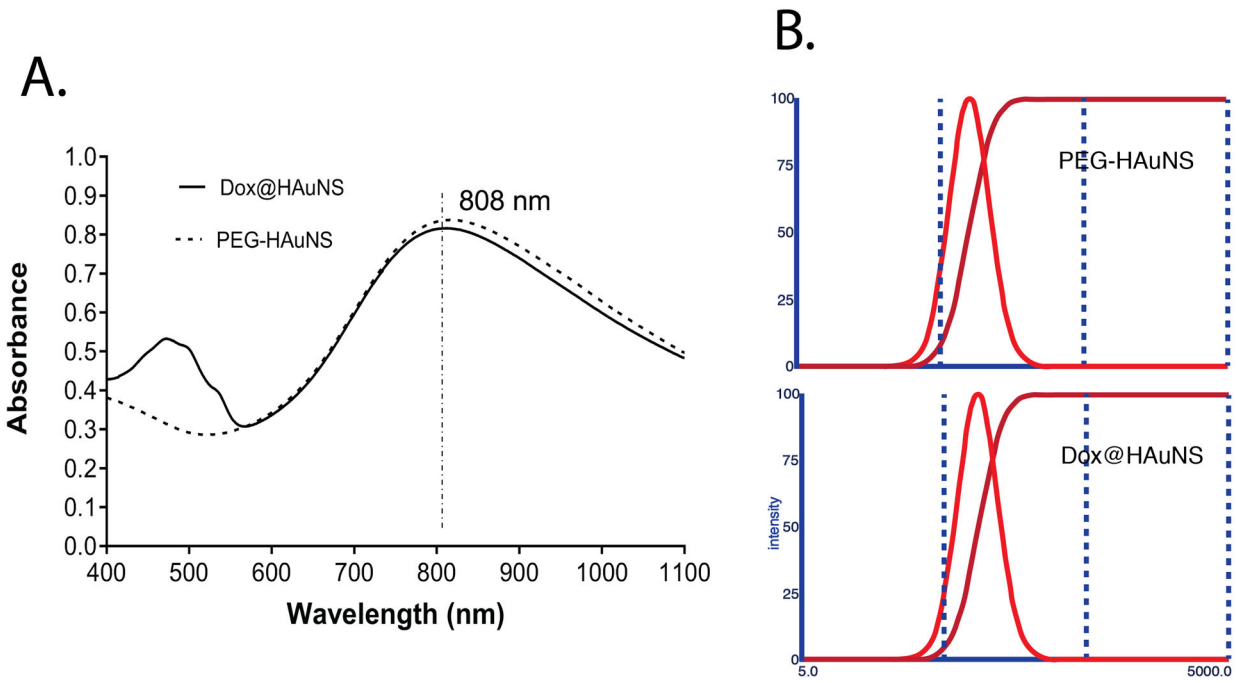


**Figure 1. Characterization of HAuNS nanoparticles.**

(**A**) Absorption spectra of PEG-HAuNS and Dox@HAuNS. (B) Dynamic light scattering histograms of PEG-HAuNS and Dox@HAuNS.

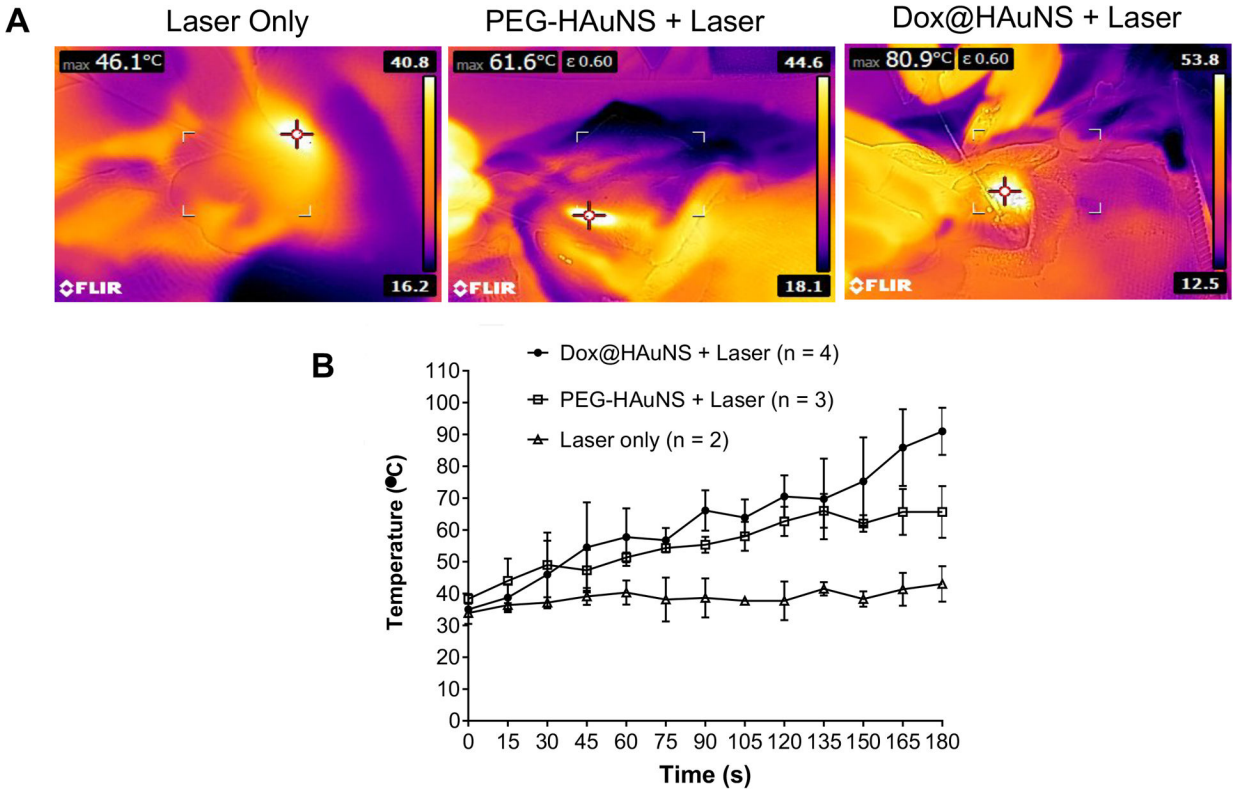


**Figure 2. Temperature elevation during laser treatment.**

(**A**) Representative infrared temperature images. (**B**) Temperature elevation as a function of treatment time. Data are presented as mean ± SD.

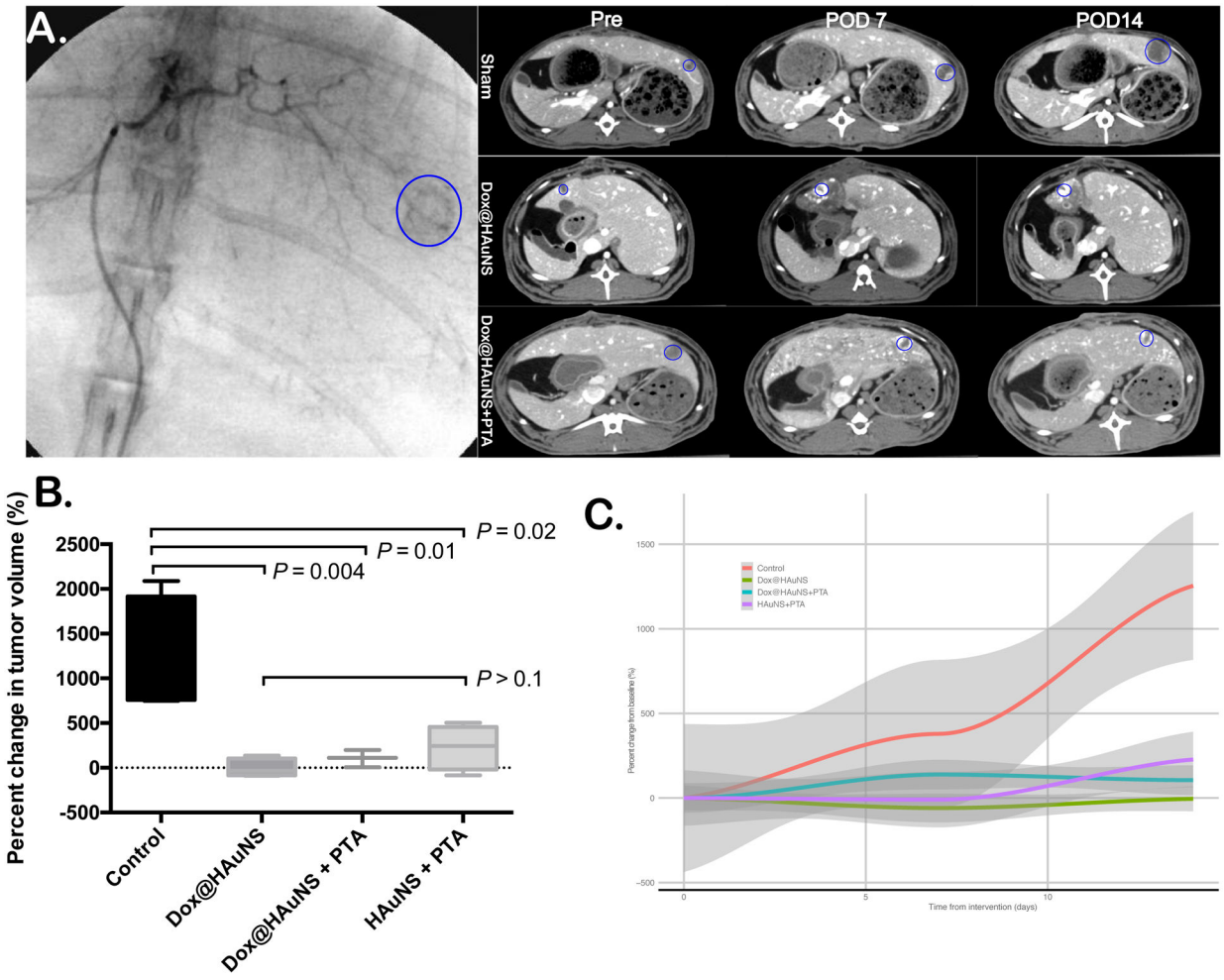


**Figure 3. CT volumetric measurements.**

(**A**) Representative angiogram and CT images of rabbits before and after laser treatment from a control rabbit (top panel) and a rabbit received intraarterial injection of Dox@HAuNS (bottom panel). Tumors are circumscribed by blue ellipses. (**B**) Percent change in tumor volume as measured by CT at POD14 compared to pre-procedure CT. Data are expressed as mean ± interquartile range. (**C**) Time course of percent change from baseline for tumors across the treatment groups. Grey zones represent 95% confidence intervals.

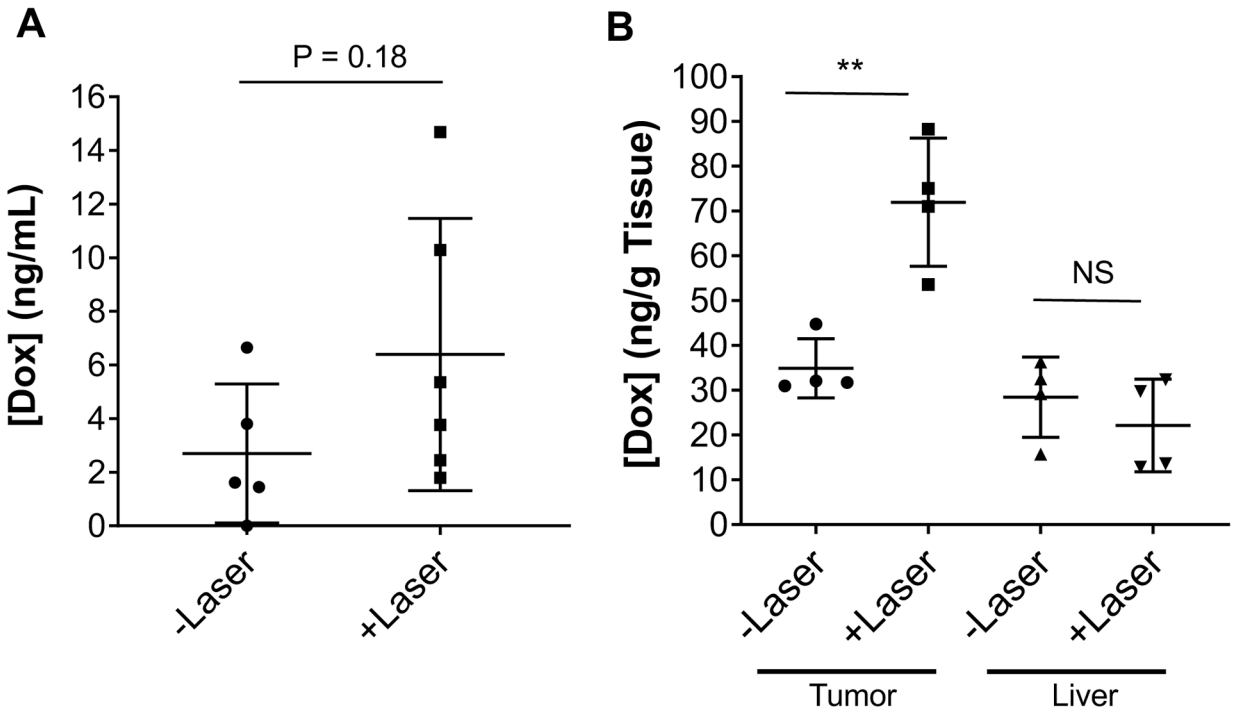


**Figure 4. Quantification of Dox concentration in tissues after Dox@HAuNS injection by HPLC.**

(**A**) Plasma Dox concentration at 1 h post treatment. (**B**) Concentration of Dox in the tumor and the liver adjacent to the tumor collected at 14 days post treatment. Data are presented as mean ± standard deviation.

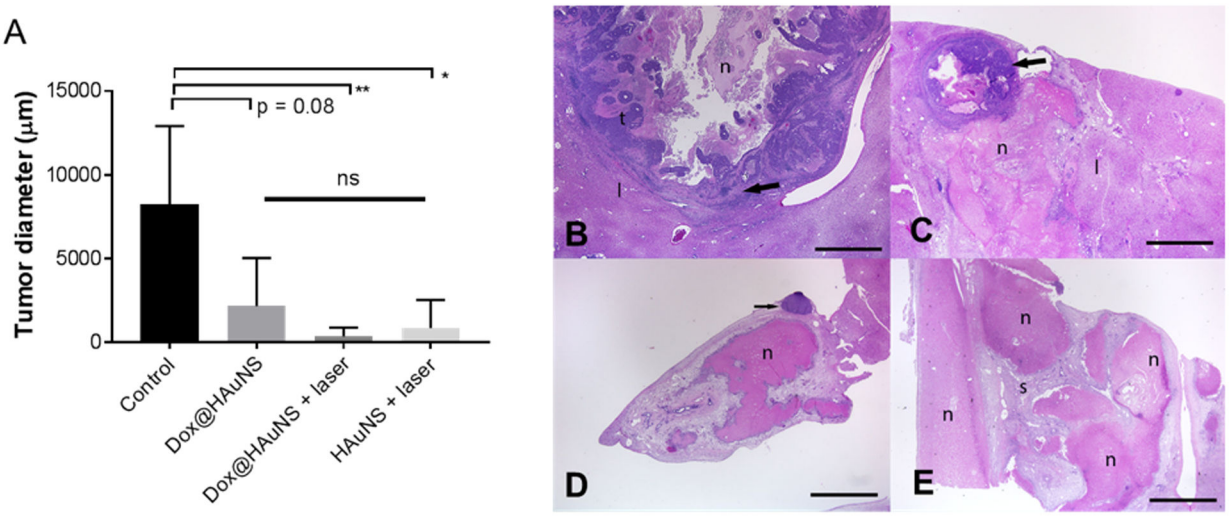


**Figure 5. Treatment response by histological examinations.**

(**A**) Tumor size measured from micrographic images of H&E stained liver/tumor tissues acquired at low magnification. Data are presented as mean ± SD. *, $p<0.05$; **, $p<0.01$ (student's t-test). (**B–E**) Representative low magnification (12.5X) photomicrographs of H&E stained tumor tissues indicating response after treatments with Dox@HAuNS + laser. (**B**) Untreated tumor from a control rabbit. A well-demarcated tumor (t) is surrounded by a layer of inflammation and fibrosis (arrow), has marked central necrosis (n), and compresses adjacent liver (l). (**C,D**) Demonstrating partial destruction of tumors from a treated rabbit. Note the areas of necrotic tumor and liver parenchyma with residual tumor (arrows). (**E**) Demonstrating complete destruction of a tumor along with ischemic necrosis of adjacent liver (n) from another treated rabbit. Only nodules of inflammation and scar tissue (s) remain. Bars = 2 mm.

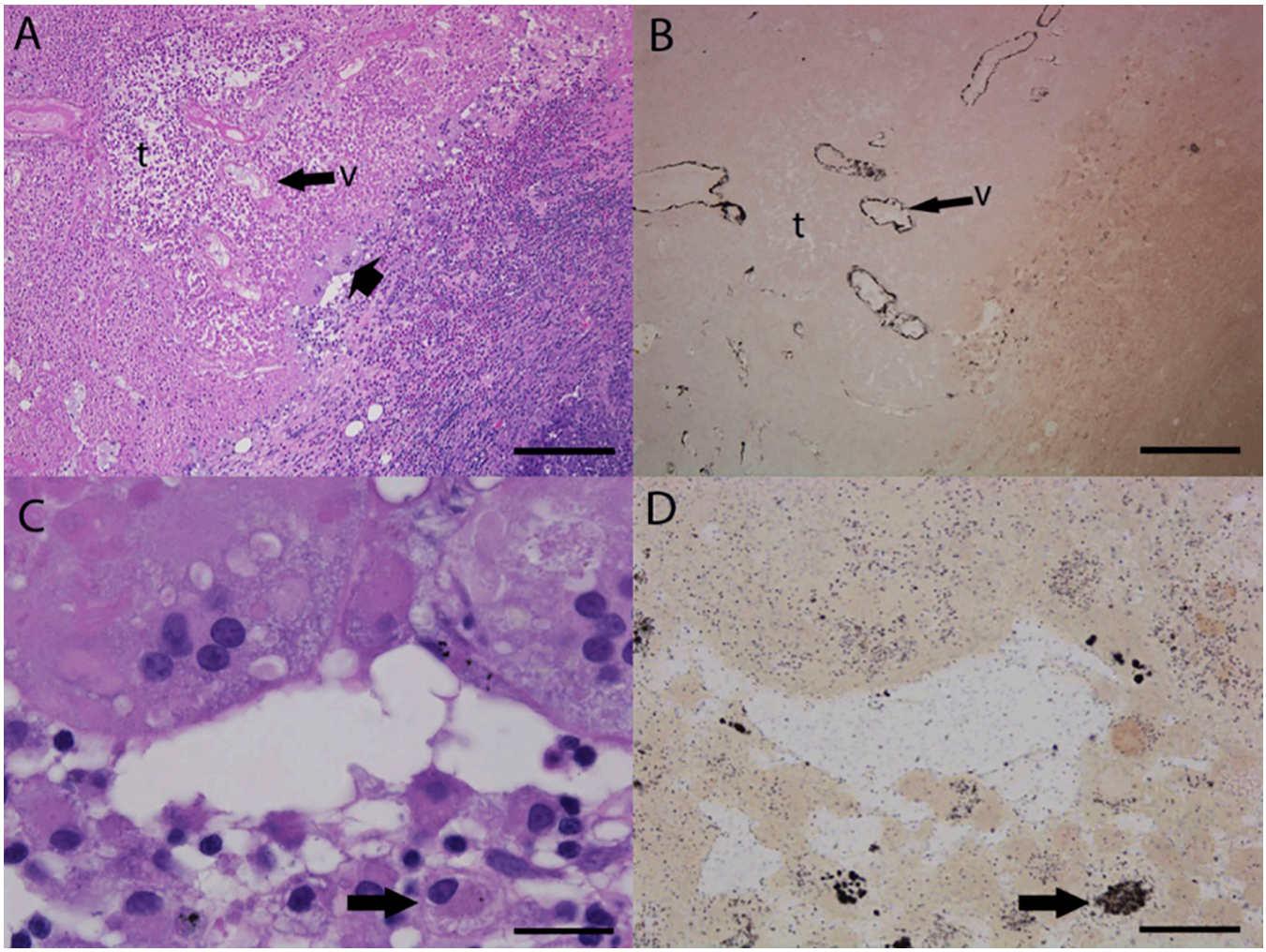


**Figure 6. Tissue Distribution of gold nanoparticles in necrotic tumor after treatments with Dox@HAuNS + laser.**

Representative photomicrographs of serial sections of necrotic tumor from DOX@HAuNS + laser-treated liver and stained with hematoxylin and eosin (**A,C**) or silver enhancer stain with neutral red counterstain for lysosomes (**B,D**). (**A,B**) Gold nanoparticles (black) were present in the necrotic wall of tumor vessels (v) in the inflammatory zone surrounding necrotic regions of VX2 tumor (t). Magnification is 50X, with bars = 500 μm. (**C,D**) Gold nanoparticles were accumulated in macrophages and multinucleated giant cells (arrows). Magnification is 400X with bars = 50 μm.